Journal of Pharmaceutical and Biomedical Analysis 52 (2010) 280–288

Contents lists available at ScienceDirect

Journal of Pharmaceutical and Biomedical Analysis

journal homepage: www.elsevier.com/locate/jpba

Molecular spectroscopic studies on the interaction between Ractopamine and bovine serum albumin

Qiulan Zhang [a], Yongnian Ni [a,b,*], Serge Kokot [c]

[a] State Key Laboratory of Food Science and Technology, Nanchang University, Nanchang, Jiangxi 330047, China
[b] Department of Chemistry, Nanchang University, Nanchang, Jiangxi 330047, China
[c] School of Physical and Chemical Sciences, Queensland University of Technology, Brisbane, Queensland 4001, Australia

ARTICLE INFO

Article history:
Received 7 August 2009
Received in revised form
28 December 2009
Accepted 5 January 2010
Available online 15 January 2010

Keywords:
Ractopamine
Bovine serum albumin
Molecular spectroscopy
Interaction
Multivariate curve resolution-alternating least squares

ABSTRACT

To investigate the interaction between Ractopamine (RAC), an animal growth promoter, and bovine serum albumin (BSA), three spectroscopic approaches (fluorescence, UV–vis and FT-IR) and three different experiments (two mole-ratio and a Job's methods) were used to monitor the biological kinetic interaction procedure. The Stern–Volmer quenching constants K_{SV}, the binding constants K_a, and the number of binding sites n at 298, 301 and 304 K were evaluated by molecular spectroscopic approaches. The values of enthalpy ($-13.47\ kJ\ mol^{-1}$) and entropy ($78.39\ J\ mol^{-1}\ K^{-1}$) in the reaction indicated that RAC bound to BSA mainly by electrostatic and hydrophobic interaction. The site markers competitive experiments indicated that the binding of RAC to BSA primarily took place in site I. The spectra data matrix was further investigated with multivariate curve resolution-alternating least squares (MCR-ALS), and the concentration profiles and the pure spectra for three species (BSA, RAC and RAC-BSA) existed in the kinetic interaction procedure, as well as the apparent equilibrium constants, were obtained.

1. Introduction

Ractopamine (RAC), originally developed to treat respiratory diseases, was found to have an important side effect of causing a significant reduction in fat levels and a dramatic increase in the amount of muscling when administered to animals in high doses [1]. It is licensed for use as an animal growth promoter in more than 20 countries worldwide, including the United States and Canada, but is either not licensed or prohibited by over 150 others, including those within the European Union, because of their well-documented adverse effects on human health, such as cardiovascular and central nervous diseases, caused by food poisoning associated with the residues in livers. But RAC was the first β-agonist approved (2003) by the US Food and Drug Administration (FDA) for use in cattle finishing diets, and the FDA (2003) [2] reported that supplementing RAC (10 or 20 ppm) during the final stages of finishing did not affect palatability of beef from mixed-breed steers and heifers [3]. Therefore, the view is very contradictory from different countries, and generally consumers consider chemical growth promoter residues as unwholesome and unwelcome constituents in food. Though there are many researches on how to detect the quantity of RAC in animals [4,5], little work has been done to search the poisonous and pharmacology adverse effect [6]. Thus, because of the requirements of providing quality assurance for the consumer and satisfying legal testing obligations, the interaction between residues of the drug at low concentrations and proteins can not only provide useful information for appropriately understanding the toxicological action, but also illustrate its binding mechanism at a molecular level.

In this work, the investigation of bovine serum albumin (BSA) with RAC was carried out in aqueous solution at physiological conditions using fluorescence, UV–vis and FT-IR spectral approaches. Spectroscopic evidence regarding the drug binding mode, the association constant and the change of protein secondary structure are provided. Furthermore, the chemometrics method, multivariate curve resolution-alternating least squares (MCR-ALS) [7], was applied to resolve the two-way UV–vis and fluorescence spectral data so as to improve the understanding of complex kinetic processes and extract the equilibrium profiles of the reacting species.

2. Material and methods

2.1. Apparatus

Fluorescence spectra for samples were measured on a Perkin–Elmer LS-55 spectrofluorometer equipped with a thermo-

* Corresponding author. Tel.: +86 791 3969500; fax: +86 791 3969500.
E-mail address: ynni@ncu.edu.cn (Y. Ni).

0731-7085/$ – see front matter © 2010 Elsevier B.V. All rights reserved.
doi:10.1016/j.jpba.2010.01.006

static bath (Model ZC–10, Ningbo Tianheng Instruments Factory, China) and a 1.0 cm quartz cuvette. The excitation and emission slits were set at 10 nm, while the scanning rate was 1500 nm min^{-1}. The FL WinLab software (Perkin–Elmer) was used to correct the measured data. The UV–vis spectra were measured on an Agilent 8453 UV–vis spectrophotometer. FT-IR spectra were measured on a Thermo Nicolet 380 FT-IR spectrometer equipped with a deuterated triglycine sulfate (DTGS) detector in the rage of 4000–400 cm^{-1}. The web-based MCR-ALS programs [8] were used to process the collected spectral data if necessary. All the measurements were carried out at room temperature (25 ± 0.5 °C).

2.2. Materials

A stock solution of 1×10^{-3} mol L^{-1} Ractopamine hydrochloride (Sigma, the purity is not less than 95.1%) was prepared by dissolving its crystals (0.0169 g) in 50 mL distilled water. BSA (2×10^{-3} mol L^{-1}) was prepared by dissolving 1.36 g of the purified protein (M = 68,000 Da; The Bomei Biological Co. Ltd., Hefei) in 10 mL 50×10^{-3} mol L^{-1} sodium chloride solution and stored at 4 °C. Its purity was 99% based on a reference absorbance value of 0.667 at 278 nm for 1.0 g L^{-1} pure BSA [9]. Essentially fatty acid free HSA was obtained from Sigma Chemical Company (St. Louis, USA). The solution of HSA (1×10^{-3} mol L^{-1}) was prepared by dissolving 0.660 g in 10 mL 50×10^{-3} mol L^{-1} sodium chloride solution based on its molecular weight of 66,000. Warfarin (Medicine Co. Ltd., Shanghai) and ibuprofen (Baike Hengdi Pharmaceutical Co. Ltd., Hubei) stock solutions (2.5×10^{-3} mol L^{-1}) were prepared by dissolving the accurately weighed appropriate amounts of each compound and dissolving in water above. The solution was then diluted to the required volume with distilled water in practical use. All experimental solutions were adjusted with the Tris–HCl ((hydroxy methyl) amino methane–hydrogen chloride) buffer of pH 7.4. Other chemicals were of analytical grade reagents, and doubly distilled water was used throughout.

2.3. Procedures

2.3.1. Fluorescence and absorbance spectra

Fluorescence spectra of BSA (3.33×10^{-8} mol L^{-1}) and HSA (3.33×10^{-8} mol L^{-1}) in presence of RAC (0–1.33×10^{-7} mol L^{-1}, with an interval of 1.67×10^{-8} mol L^{-1}) were recorded at 298, 301 and 304 K. An excitation wavelength of 280 nm was chosen and the emission wavelength was recorded from 200 to 450.5 which was used to calculate the thermodynamic and binding parameters of RAC and BSA/HSA systems. Synchronous fluorescence spectra (SFS) of BSA (1.67×10^{-7} mol L^{-1}) in the presence of RAC were measured (λ_{ex} = 200–350 nm; $\Delta\lambda$ = 60 and 15 nm) at pH 7.4, the concentration of RAC was increased from 0 to 2.67×10^{-7} mol L^{-1} at an interval of 3.34×10^{-8} mol L^{-1} (total 9 samples).

2.3.2. FT-IR spectroscopy

FT-IR spectra are taken via the attenuated total refection (ATR) method with resolution of 4 cm^{-1} and 32 scans (range of 400 and 4000 cm^{-1}). The spectra of the buffer solution was firstly collected and then subtracted the spectra of buffer from the spectra of sample solution to get the FT-IR spectra of the protein.

2.3.3. The experiments to get the expanding data matrix

Three separate experiments were carried out in the Tris–HCl buffer of pH 7.4, and the experimental conditions and necessary variables are listed in Table 1.

Experiment 1 (mole-ratio method): the concentration of BSA was kept constant (3.33×10^{-8} mol L^{-1}), and different amounts (0–1.00×10^{-7} mol L^{-1}, at 5.00×10^{-9} mol L^{-1} interval) of RAC were added to the solution. Experiment 2 (mole-ratio method): the concentration of RAC was kept constant (6.67×10^{-8} mol L^{-1}) and different amounts of BSA were added with a range of 0–6.67×10^{-8} mol L^{-1} at an interval of 3.33×10^{-9} mol L^{-1}. Experiment 3 (Job's method, sometimes called continuous variation method): the concentration of RAC was kept change from 3.33×10^{-8} mol L^{-1} to 0 and different amounts of BSA were added in the range of 0–3.33×10^{-8} mol L^{-1}. The ratios of $r_{RAC:BSA}$ and $r_{BSA:RAC}$ were ranged from 1.0 to 0 and 0 to 1.0, respectively.

The solutions used in experiments 1–3 were prepared with 3.0 mL of pH 7.4 Tris–HCl buffer containing appropriate amounts of BSA and RAC. The total added volume (BSA and RAC) was less than 0.1 mL, so the volume variation was thus negligible. Titrations were performed manually using suitable micropipettes. The mixed solution was shaken thoroughly and equilibrated for 10 min and then the molecular fluorescence (200–450.5 nm) and UV–vis (200–450 nm) spectra were recorded at every 0.5 and 1 nm, respectively. Thus, six data matrices D_{UV}^{BSA}, D_{F}^{BSA} (experiment 1) D_{UV}^{RAC}, D_{F}^{RAC} (experiment 2) and D_{UV}^{Var}, D_{F}^{Var} (experiment 3) can be obtained, these column-wise and row-wise data matrices with two different measuring approaches for three different experiments were combined and expanding data matrix was obtained.

2.3.4. Fluorescence spectra in the presence of the site markers

In order to identify the binding site of RAC on BSA, warfarin and ibuprofen were used as the markers for sites I and II, respectively.

Method 1: the marker was added to the mixture of RAC and BSA, the ratio of $r_{RAC:BSA}$ was kept at 2, but the concentrations of the site marker I (warfarin) for one series, and II (ibuprofen) for the other series, were varied.

Method 2: site I marker of warfarin, with different concentration, was added to a series of test tubes containing BSA of 3.33×10^{-8} mol L^{-1}, total six solutions with different molar ratios of $r_{warfarin:BSA}$ (0–5) were prepared, and then RAC was added to these six tubes at different concentrations (from 0 to 1.33×10^{-7} mol L^{-1} at 1.67×10^{-8} mol L^{-1} interval, total 9 times, respectively. Fluorescence spectra were measured as previously described. The binding constants, K_a, of the RAC to BSA were then calculated according to the double-logarithm equation.

2.4. Theoretical background for chemometrics methods

Multivariate curve resolution-alternating least squares (MCR-ALS) has been used for the resolution of multiple component responses in unknown mixtures. UV–vis, fluorescence, near-infrared reflectance (NIR), HPLC and circular dichroism (CD) were used with MCR-ALS optimization step described elsewhere [10]. A short description of the MCR-ALS is given here.

The multivariate curve resolution model can be written as Eq. (1):

$$\boldsymbol{D} = \boldsymbol{C}\boldsymbol{S}^{T} + \boldsymbol{E} \quad (1)$$

The bilinear method to resolve an experimental data matrix $\boldsymbol{D}$ ($M \times N$) into the product of a column matrix $\boldsymbol{C}$ ($M \times F$) usually associated with concentration profiles, and a matrix of row profiles $\boldsymbol{S}^{T}$ ($F \times N$), usually associated with spectra. The superscript "T" means the transpose of matrix $\boldsymbol{S}$, where pure spectra are column profiles. $\boldsymbol{E}$ is the matrix of residuals and ideally should be close to the experimental error. M is the number of spectra recorded throughout the process and N is the number of the instrumental responses measured at each wavelength. The number of species, F, is directly related with the number of main components in matrix $\boldsymbol{D}$. This number is estimated by rank analysis, using singular value decomposition (SVD), principal component analysis (PCA), or some related techniques based on factor analysis, such as evolving factor analysis (EFA) [11] or pure-variable detection methods like SIMPLISMA

Table 1
The experiments to build up the extension matrixes.

Experiment	c_{BSA} (mol L^{-1})	c_{RAC} (mol L^{-1})	Number of spectra	Data matrix	
1	3.33×10^{-8}	$0–1 \times 10^{-7}$	21	D_{UV}^{BSA}	D_{F}^{BSA}
2	$0–6.67 \times 10^{-8}$	6.67×10^{-8}	21	D_{UV}^{RAC}	D_{F}^{RAC}
3	$3.33 \times 10^{-8}–0$	$0–33.3 \times 10^{-8}$	21	D_{UV}^{Var}	D_{F}^{Var}

For each experiment, UV–vis (200–450 nm, N_{UV} = 251 wavelength points), and fluorescence (200–450.5 nm, N_F = 502 wavelength points) were measured.

[12]. Once F is obtained, an initial estimate of their concentration profiles is obtained from EFA plot and generally can be submitted as the initial value for further calculation.

Recently, a powerful extension of MCR-ALS was developed to deal with multiple data matrices simultaneously [7,13,14], and it is possible to resolve several independent samples and/or several measurement techniques by augmenting the input matrix appropriately. In this paper, there were three types of experiment and two types of spectroscopic method, so a total of six data matrices were obtained. The data arrangement evaluated by the extended MCR-ALS analysis can be represented as following:

$$\begin{bmatrix} \boldsymbol{D}_{UV}^{BSA} & \boldsymbol{D}_{F}^{BSA} \\ \boldsymbol{D}_{UV}^{RAC} & \boldsymbol{D}_{F}^{RAC} \\ \boldsymbol{D}_{UV}^{Var} & \boldsymbol{D}_{F}^{Var} \end{bmatrix} = \begin{bmatrix} \boldsymbol{C}^{BSA} \\ \boldsymbol{C}^{RAC} \\ \boldsymbol{C}^{Var} \end{bmatrix} \times \begin{bmatrix} \boldsymbol{S}_{UV}^{T} & \boldsymbol{S}_{F}^{T} \end{bmatrix} + \begin{bmatrix} \boldsymbol{E}_{UV}^{BSA} & \boldsymbol{E}_{F}^{BSA} \\ \boldsymbol{E}_{UV}^{RAC} & \boldsymbol{E}_{F}^{RAC} \\ \boldsymbol{E}_{UV}^{Var} & \boldsymbol{E}_{F}^{Var} \end{bmatrix} \quad (2)$$

where the superscripts BSA, RAC and Var refer to experiments 1, 2 and 3 in Section 2.3.3, respectively. The first term is the augmented experimental data matrix, which contains all the spectroscopic data from the three different experiments. [$\boldsymbol{C}^{BSA}$, $\boldsymbol{C}^{RAC}$, and $\boldsymbol{C}^{Var}$] is the data matrix containing the recovered MCR-ALS concentration profiles for the three experiments and [$\boldsymbol{S}_{UV}$, $\boldsymbol{S}_{F}$]^T is the data matrix of the recovered pure spectra for each species. The last term is the residual variance. A number of six individual data matrices are simultaneously analyzed using Eq. (2).

This kind of synchronous data analysis is much more vigorous as compared with those described by Eq. (1) and allows for the improvement of resolution of very complex data structures, as those found in articles [7,15]. The approach assembles the profits of both augmentations previously described and gives more reliable solutions, eventually removing rotational ambiguities and rank-deficiency problems. The resolution of experimental spectral expanding data matrix $\boldsymbol{D}$ consists of several steps as described in the literature [16].

3. Results and discussion

3.1. Principles of fluorescence quenching

Fluorescence quenching is the decrease of the quantum yield of fluorescence from a fluorophore induced by a variety of molecular interactions, such as excited-state reactions, molecular rearrangements, energy transfer, ground-state complex formation, and collisional quenching [17]. Dynamic quenching depends upon diffusion, since higher temperature results in larger diffusion coefficients; the bimolecular quenching constants are expected to increase with increasing temperature. In contrast, increased temperature is likely to result in decreased stability of complexes, and thus lower the static quenching constants [18]. The possible quenching mechanism can describe by the Stern–Volmer Eq. (3):

$$\frac{F_0}{F} = 1 + K_q \tau_0 [Q] = 1 + K_{SV}[Q] \quad (3)$$

where F_0 and F represent the fluorescence intensities in the absence and in the presence of quencher, respectively. K_q is the quenching rate constant of the bimolecular, K_{SV} is the dynamic quenching constant, τ_0 the average lifetime of the bimolecular without quencher, and [Q] is the concentration of quencher. In order to confirm the quenching mechanism, the procedure of the fluorescence quenching was assumed to be a dynamic quenching process. Table 2 summarizes the calculated K_{SV} at each temperature studied, the results show that the Stern–Volmer quenching constant K_{SV} is inversely correlated with temperature, which indicate that the probable quenching mechanism of RAC-BSA binding reaction is initiated by compound formation rather by dynamic collision [19]. According to the literature [17], for dynamic quenching, the maximum scatter collision quenching constant of various quenchers with biopolymers is 2.0×10^{10} L mol^{-1} s^{-1}. Obviously, the rate constant of protein quenching procedure initiated by RAC is larger than the K_q of the scatter procedure. This also means that in this biological kinetic system, the quenching is not initiated by dynamic collision but from the formation of a complex, which further prove that a complex of RAC-BSA has been born.

3.2. Binding constant and binding sites

Since the fluorescence quenching behavior of BSA deduced by RAC was a static quenching process, the association constants K_a, and the number of binding sites n, can be obtained from the double-logarithm curve based on the following equation [20]:

$$\log \left[\frac{(F_0 - F)}{F}\right] = \log K_a + n \log [Q] \quad (4)$$

The fluorescence quenching intensities of BSA at 350 nm were measured, and the corresponding results calculated by Eq. (4) were listed in Table 2. The decreasing trend of K_a with the increasing temperature was in accordance with K_{SV} and K_q dependence on the temperature as mentioned above, which indicates that RAC-BSA would be partly decomposed when the temperature was increased. The correlation coefficients are larger than 0.992, indicating that the interaction between RAC and BSA agrees well with the site-binding model underlined in Eq. (4), and it suggests that there is a strong binding force between RAC and BSA. The values of n approximately equal to 1 indicate the existence of just one high affinity of binding site in BSA for RAC. The strong binding force and one high affinity binding site are identical with the extraction information from MCR-ALS method which is of particular significance to pave the way for a better understanding of the drug–protein interaction.

3.3. Type of interaction force between RAC and BSA

Thermodynamic parameters for a binding interaction can be used as a major evidence to investigate the nature of intermolecular forces. If the enthalpy changes (ΔH) do not vary significantly over the temperature range studied, the values of ΔH and ΔS can be estimated from the van't Hoff equation [21]:

$$\ln K = -\frac{\Delta H}{RT} + \frac{\Delta S}{R} \quad (5)$$

and the free energy changes (ΔG) at different temperatures can be calculated according to the following:

$$\Delta G = \Delta H - T\ \Delta S \quad (6)$$

where K is analogous to the effective quenching constants, K_a, at the corresponding temperature and R is the gas constant. According to the binding constants of RAC to BSA obtained at three temperatures

Table 2
Thermodynamic and binding parameters of RAC and BSA systems.

T (K)	K_{SV} ($\times 10^6$ L mol^{-1})	R^2	K_a ($\times 10^6$ L mol^{-1})	n	ΔG (kJ mol^{-1})	ΔH (kJ mol^{-1})	ΔS (J mol^{-1} K^{-1})
BSA							
298	2.47	0.9962	2.86	0.9436	−36.83	−13.47	78.39
301	2.40	0.9970	2.66	0.9564	−37.14		
304	2.15	0.9926	2.31	0.9926	−37.28		
HSA							
298	1.98	0.9990	5.86	0.8421	−38.61	−33.33	17.72
301	1.39	0.9963	4.91	0.8065	−38.17		
304	1.14	0.9940	4.25	0.8592	−37.81		

above, the thermodynamic parameters were obtained from Eq. (5) and were listed in Table 2. The negative ΔH indicated that the formation RAC-BSA complex was an exothermic reaction procedure, and the negative sign for ΔG means that the binding process was spontaneous. Ross and Subramanian [21] have characterized the sign and magnitude of the thermodynamic parameter associated with various individual kinds of interaction that may take place in protein association process. Thus, from the thermodynamic characteristics summarized, the negative enthalpy (−13.47 kJ mol^{-1}) and positive entropy (78.93 J mol^{-1} K^{-1}) values indicate that the electrostatic and hydrophobic interactions played a major role in the interaction and contributed to the stability of the complex.

3.4. Binding property of the RAC to HSA

BSA structure is similar to HSA in 76%. To further study the interaction of the drug with the serum albumin, the binding parameters were also investigated by fluorescence spectroscopy as described in Section 2.3.1 and the estimated parameters are listed in Table 2. Results showed that RAC quenched the fluorescence of HSA through static quenching mechanism. The values of n revealed the presence of a single class of binding site on HSA for RAC. The thermodynamic parameters indicated that the acting forces between RAC and HSA was also mainly electrostatic interactions. The K_{SV} and K_a of RAC with HSA were the same order of magnitude as that of RAC with BSA. Therefore, in this paper, BSA was selected as the protein model because of its low cost, ready availability, and unusual ligand-binding properties [22].

3.5. Study of the conformation of BSA upon addition of RAC

The synchronous fluorescence spectra (SFS) can provide the information on the molecular micro-environment, particularly in the vicinity of the fluorophore functional groups [23]. To investigate the structural change of BSA by the addition of RAC, SFS for BSA with various concentrations of RAC were measured. According to Miller [24], the difference between excitation and emission wavelength ($\Delta\lambda = \lambda_{em} - \lambda_{ex}$) reflects the spectra of a different nature of chromophores, with large $\Delta\lambda$ values such as 60 nm, the synchronous fluorescence of BSA is characteristic of tryptophan residue and the small $\Delta\lambda$ values such as 15 nm is characteristic of tyrosine. The SFS of BSA with various concentrations of RAC were recorded at $\Delta\lambda$ of 60 and 15 nm (Fig. 1a and b). With the addition of RAC the intensity of tyrosine was increased and a blue shift (Fig. 1b) was observed. Contrary, the tryptophan fluorescence emission was decreased regularly with increasing concentration of RAC, and also there was a blue shift (Fig. 1a). The fluorescence spectra may represent that the conformation of BSA changed, leading to the polarity around tyrosine and tryptophan residues weakened and the hydrophobicity strengthened [25].

It concludes that RAC may affect both the tyrosine and tryptophan residues present in BSA, through dehydrating esterification, two products were found (Scheme 1). Because of the tyrosine product containing two aromatic hydroxyl groups, aromatic hydroxyl group push electronic to the benzene, so the synchronous fluorescence spectra increased. Because the fluorescence quenching mainly contributed by the tryptophan residue, the influence of tyrosine can be negligible.

Additional evidence regarding the changes of BSA's secondary structures induced by RAC binding came from FT-IR spectroscopy results. Since infrared spectra of proteins exhibit a number of amide bands, which represent different vibrations of the peptide moiety. For all the amide modes of the peptide group, the single most widely used one in studies of protein secondary structure is amide I. This vibration mode originates from the C=O stretching vibration of the amide group (coupled to the in-phase bending of the N–H bond and the stretching of the C–N bond) and gives rise to infrared bands in the region between approximately 1600 and 1700 cm^{-1} [26]. In Fig. 2, the FT-IR spectra of the RAC-free and bound form of BSA with its difference absorption spectrum were obtained in order to monitor the intensity variations of these vibrations. From Fig. 2, it is concluded that the secondary structure of BSA was changed

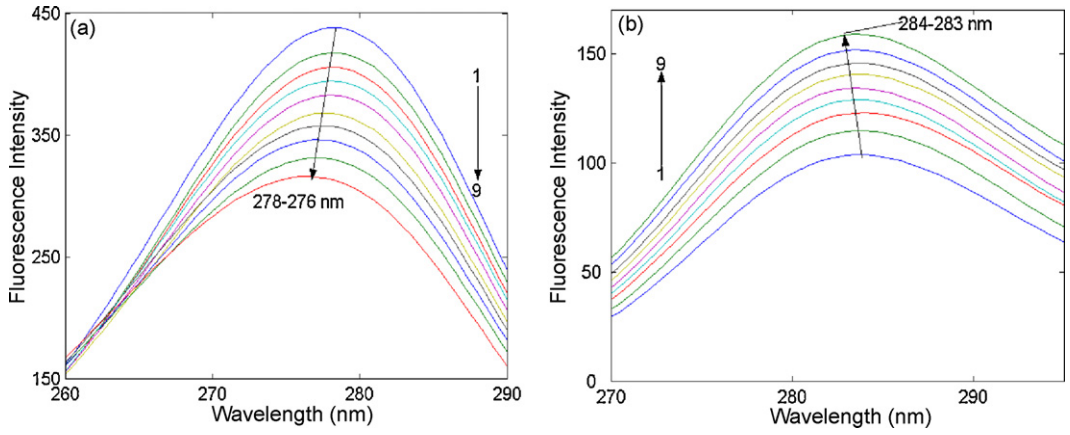

Fig. 1. The synchronous fluorescence spectra of BSA by addition of RAC ($\Delta\lambda = 60$ and $\Delta\lambda = 15$ nm, $c_{BSA} = 1.67 \times 10^{-7}$ mol L^{-1}, and [RAC]:[BSA] = 0.0, 0.2, 0.4, . . ., 1.6 for curves 1–9, respectively).

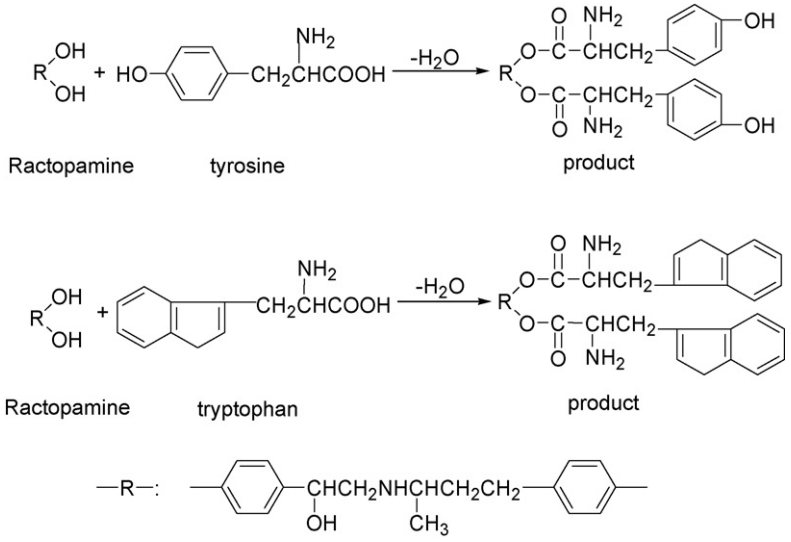

Scheme 1. Mechanism for the interaction of Ractopamine with BSA.

because the peak position of amide I band (1660 cm^{-1}) and amide II band (1544 cm^{-1}) in the IR spectrum of BSA has evidently shifted to 1656 and 1541 cm^{-1}, respectively, and their peak intensity are also changed. The reduction of α-helices and β-sheet in favor β-turn and random coil structures is indicative of a partial unfolding of the protein in the presence of RAC.

3.6. The kinetic binding procedure of between RAC and BSA with different experiments

The interaction between RAC and BSA was studied by fluorescence and UV–vis spectra in pH 7.4 Tris–HCl buffer. Fig. 3 shows the spectroscopic data obtained from the experiments summarized in Table 1. Fluorescence of BSA originates from tryptophan, tyrosine, and phenylalanine residues, where the intrinsic fluorescence of BSA mainly contributes by the tryptophan residue alone. Fig. 3a–c shows the fluorescence spectra gained from the above three different titrations (see Section 2.3.3). Fig. 3d–f corresponds to UV–vis spectra. Fig. 3a displays the emission spectra of BSA in the presence of various concentrations of RAC. It is observed that the fluorescence intensity of BSA at 350 nm decreased regularly with the increasing concentration of added RAC, but when the ratio of $r_{RAC:BSA}$ was nearly to 2.1, the fluorescence intensity decreased little. An increase in the fluorescence intensity of RAC at 310 nm assigned that RAC appeared. In addition, an isoactinic point formed at 340 nm, which manifested equilibrium between the free RAC and the molecule bound to BSA. Obviously, a slight blue shift was discovered, it might be referred to that the intermolecular forces involved to maintain the secondary structure, which could be altered and resulted in the conformational changes of tryptophan and tyrosine micro-region caused by interaction of RAC with BSA [27]. Fig. 3d presents the UV–vis spectra of experiment 1, which shows peaks at 278 nm (curve 1) and a blue shift which floated from 278 nm to the drugs characteristic absorbance peak (274 nm) can be observed and the another spectral peak at 222 nm also got more higher with the continuous addition of RAC. Fig. 3b shows the emission spectra of RAC in the presence of BSA with various concentrations. With the titration of BSA, the emission spectrum of RAC (curve 1) at 310 nm disappeared in curve 10 when the ratio of $r_{RAC:BSA}$ was approximate to 2 and a new emission peak appearing at 350 nm assigned with the addition of BSA. UV–vis spectrum (curve 1) of experiment 2 (Fig. 3e) shows at 274 nm, there is a red shift (from 274 to 278 nm) can be observed with the increasing of BSA (curves 1–10, [RAC]:[BSA] = 0–2). This indicates the changes of the environment of the tryptophanyl residues of BSA, the peptides strand less extends, and the hydrophobicity is increased. Moreover, from curves 11 to 21 no peak change can be observed for peak at 278 nm, which may demonstrate that the BSA-RAC kinetic system had already reached to equilibrium. The peak at 222 nm vanished with the addition of BSA. No apparent phenomenon can be observed from fluorescence and UV–vis spectra of the Job's method (see Fig. 3c and f) and no more information can be provided directly.

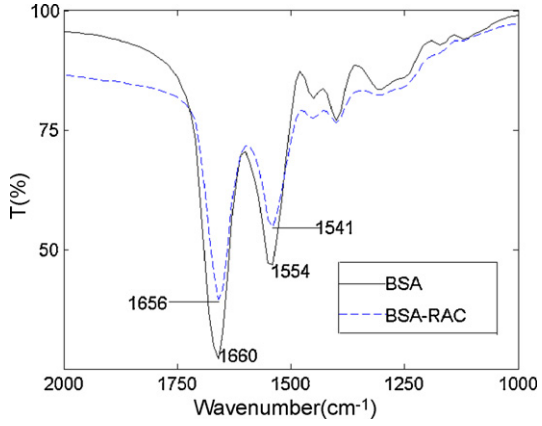

Fig. 2. The FT-IR spectra of BSA in the absence and presence of RAC.

3.7. Resolution of the overlapped spectra of RAC-BSA with the aid of MCR-ALS

Generally, both for the fluorescence and the UV–vis spectra alone (Fig. 3a–f), it is difficult to deduce the formation of a complex in the kinetic binding reaction system because of the high spectral overlap for each species. Therefore, in this work the whole set of spectroscopic data matrices (called expanded data matrix) was simultaneously resolved by the MCR-ALS to obtain useful information of the biological kinetic system, including the RAC-BSA complex, the concentration profiles, the pure spectra for each species and the calculation of the apparent equilibrium, and to explore the essence of the drug's affection on BSA.

To apply MCR-ALS, the first step was to build up the expanding data matrix by joining the individual data matrices in the way

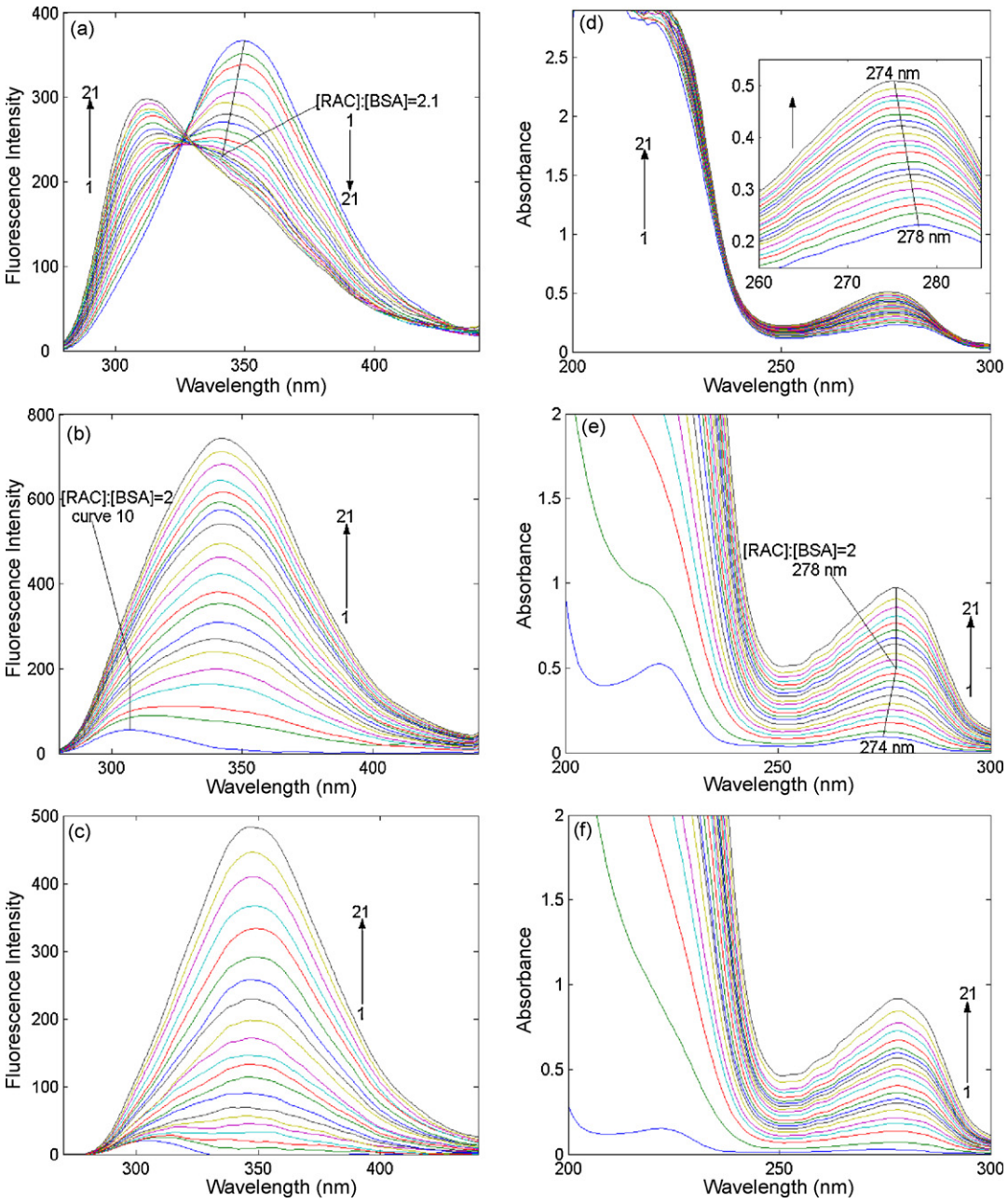

Fig. 3. Spectra obtained from different experiments. Experiment 1: (a) fluorescence (D_F^{BSA}) and (d) UV–vis (D_{UV}^{BSA}), $c_{BSA} = 3.33 \times 10^{-8}$ mol L^{-1}, RAC was added with different concentrations, ($c_{RAC} = 0$, 0.5, 1, . . ., 10×10^{-8} mol L^{-1} for curves 1–21, respectively). Experiment 2: (b) fluorescence (D_F^{RAC}) and (e) UV–vis (D_{UV}^{RAC}), $c_{RAC} = 6.67 \times 10^{-8}$ mol L^{-1} and $c_{BSA} = 0$, 3.33, 6.67, . . ., 6.67×10^{-8} mol L^{-1} for curves 1–21, respectively. Experiment 3: (c) fluorescence (D_F^{Var}) and (f) absorption (D_{UV}^{Var}), different amounts of RAC were added in the range from 3.33×10^{-8} to 0 mol L^{-1} and BSA were added in the range of 0–3.33×10^{-8} mol L^{-1} ([BSA]:[RAC] = 0.0, 0.05, 0.1,. . ., 1.0 for curves 1–21, respectively).

shown in Eq. (2), and the next step was to evaluate the number of factors which could be related to chemical species by EFA method and to estimate the initial concentration for the species existed in the kinetic binding procedure. MCR-ALS constrained optimization was then applied with an initial estimate of the concentration profiles obtained from EFA for the three species postulated. The concentrations calculated in that optimization were constrained to be positive or zero and to give unimodel profiles. Moreover, as the total concentration of RAC and BSA were known in the experiments, this information was also included as a closure constraint for the concentrations profiles.

From the finally resolved pure spectra, qualitative information about the nature of the complex was extracted. Fig. 4a–b shows the pure fluorescence and UV–vis spectra recovered for different species, which correspond to $\boldsymbol{S}_F^T$ and $\boldsymbol{S}_{UV}^T$, respectively. These obtained fluorescence and UV–vis spectra (dashed line) compared well with the measured spectra (solid line). It should be emphasized that the fluorescence and UV–vis spectra for the BSA-RAC complex (see dashed line of RAC-BSA in Fig. 4a and b), and the concentration profiles of RAC, BSA and the BSA-RAC complex in the kinetic binding procedure (see the fitted curves of BSA, RAC and RAC-BSA in Fig. 4c–e), which are difficult to obtain by conventional methods, were obtained with the use of MCR-ALS. In contrast, from Fig. 4b, a clear red shift of the maximum absorbance can be observed from free BSA to BSA-RAC binding complex and a blue shift can also be seen in the received fluorescence spectrum (see Fig. 4a) of free BSA when RAC was added, which can be ascertained that the conformation and/or the micro-

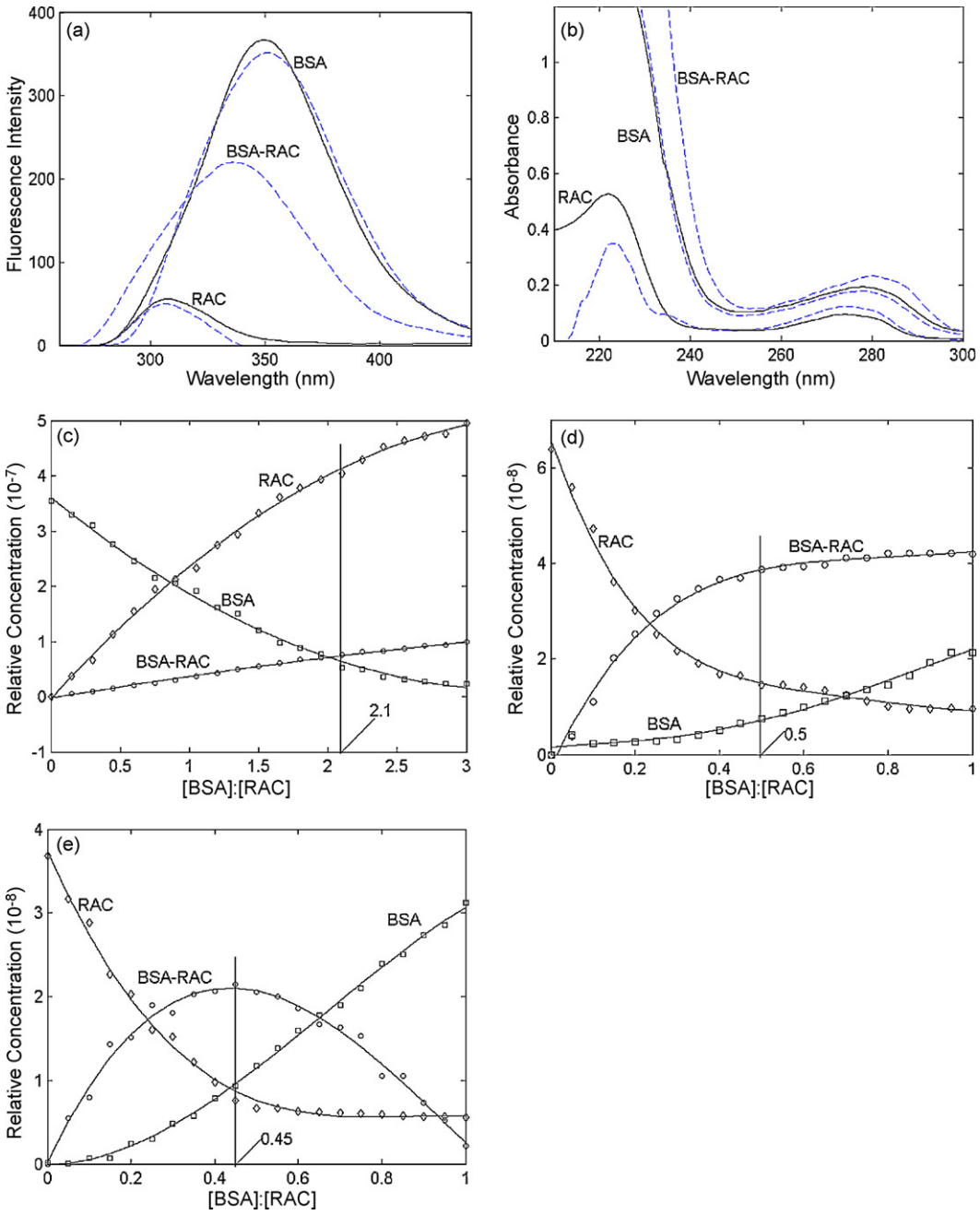

Fig. 4. Results of the simultaneous analysis of the UV–vis and fluorescence data matrices of the three experiments. Recovered UV–vis spectra (a) and fluorescence spectra (b). Recovered concentration profiles for experiment 1 (c), experiment 2 (d) and experiment 3 (f).

environment of BSA were affected by the binding of BSA with RAC.

For evaluation of the pure fluorescence and UV–vis spectra of RAC-BSA complex (see Fig. 4a and b) from the biological kinetic system (see Fig. 3a–c and d–f, respectively), it is impossible to get these two spectra without the use of expanded MCR-ALS because of the high overlap spectra of the existing species.

3.8. Estimation of the apparent formation constant (K_{app}) of the complex

The concentration profiles recovered with MCR-ALS by the mole-ratio method keeping c_{BSA} or c_{RAC} constant and for the continuous variation method are shown in Fig. 4c–e. These three plots correspond to data matrices $\mathbf{C}^{BSA}$, $\mathbf{C}^{RAC}$ and $\mathbf{C}^{Var}$, respectively. The recovered concentration profiles show the expected trends related with the different kind of experiments performed. For experiments 1 with mole-ratio method (Fig. 4c), the concentration of the intercalation complex increases slowly and reach to the equilibrium when the ratio of [RAC]:[BSA] is 2.1, while for experiments 2 (Fig. 4d), the concentration of the intercalation complex increases sharply from beginning to $r_{BSA:RAC} \sim 0.5$ and approaches to equilibrate as the concentration of BSA increased continuously. For the Job's method (Fig. 4e), the concentration of the intercalation complex reaches approximately a maximum at $r_{BSA:RAC} \sim 0.45$ and 0 at the initial and final points of the experiment, it is similar as a transient intermediate.

Furthermore, from the estimated concentration profiles, it is possible to calculate a value of the apparent formation constant (K_{app}) of the complex as following:

$$K_{app} = \frac{[\text{RAC-BSA}]}{[\text{RAC}][\text{BSA}]} \quad (7)$$

where [RAC-BSA], [RAC] and [BSA] are the estimated concentrations for the complex, free RAC and free BSA, respectively at each point of the concentration profiles. The [RAC]:[BSA] for the complex was 2.1 (Fig. 4c), and the value of K_{app} was calculated as 3.13×10^6 ($\log K_{app}$ is 6.49) according to Eq. (7). The molar ratio of [BSA]:[RAC] for the complex is 0.5 in Fig. 4d, and K_{app} was obtained as 2.76×10^6 ($\log K_{app} = 6.43$). The [BSA]:[RAC] was 0.45 (Fig. 4e), and K_{app} was 3.17×10^6 ($\log K_{app} = 6.50$). Thus, the estimates of K_{app} (BSA-RAC) obtained from three different cases were similar, which indicated that there was a strong interaction force between the RAC and BSA molecules, and the drug will exist in the blood plasma with a long time and play a profound poisonous effect [28]. From the recovered concentration profiles (Fig. 4c–e), the [RAC]:[BSA] molar ratio in the complex was approximate to 2, which indicates that at different experimental conditions there was one binding site per two base pairs [29]. Furthermore, as described above, almost equal values of 6.49, 6.43 and 6.50 were obtained for the $\log K_{app}$, and the estimate K_{app} ($2.90 \pm 0.25 \times 10^6$) was in good agreement with the one obtained by conventional method (see Section 3.2 and Table 2).

3.9. Effect of siter, warfarin and ibuprofen, on the binding of RAC to BSA

Crystal structure of BSA is a heart-shaped helical monomer composed of three homologous domains named I, II, III and each domain includes two sub-domains called A and B to form a cylinder [30]. The principal regions of ligand-binding sites on albumin are located in hydrophobic cavities in sub-domains IIA and IIIA, which exhibit similar chemical properties [31]. These two binding cavities are also referred to sites I and II according to the terminology proposed by Sudlow et al. [32]. In order to identify the β-agonist binding site on BSA, site marker competitive experiments were carried out, using drug which specially bind to a known site or region on BSA. From X-ray crystallography studies, warfarin has been demonstrated to bind to the sub-domain IIA while ibuprofen is considered as IIIA binder [33]. Then information about the RAC-BSA binding site can be gained by monitoring the changes in fluorescence of RAC bound albumin that brought about by site I (warfarin) and site II (ibuprofen) markers.

Interaction parameters of RAC with BSA indicated a quite strong binding site (see Table 2). In order to locate the RAC binding site on the BSA, the displacement of RAC bound to BSA was performed by fluorescence titration with the addition of warfarin (Section 2.3.4, method 1). The characteristic emission fluorescence of BSA at 350 nm was quenched (see Fig. 5), thus, warfarin appeared to bind at the same site as RAC. This observation supported site I as the RAC binding mode on the BSA protein. A similar fluorescence titration was also carried out for site II marker ibuprofen, and no obvious effect on the binding of RAC to BSA was observed. The displacement percentage only reached about 8% when [ibuprofen]/[BSA] = 10, which indicated the two molecules did not share a similar binding site on the BSA.

The influence of warfarin on the interactions of RAC-BSA was further investigated. RAC was gradually added to the solution of BSA and site markers held in different ratios (method 2 in Section 2.3.4). With the addition of RAC into warfarin-BSA solution, the fluorescence intensity at 350 nm of the BSA with different molar ratio warfarin ($r_{warfarin:BSA} = 0, 1, 2, \ldots, 5$) decreased gradually, indicating that the bound RAC to BSA was affected by adding warfarin. In order to facilitate the comparison of the influence of warfarin on the binding of RAC to BSA, the fluorescence quenching data of the RAC-BSA system with the presence of site marker was also analyzed using the double-logarithm equation. The binding constants of the RAC-BSA system, which can be calculated from the slope values of the plots, were listed in Table 3. Obviously, the binding constant of the RAC-BSA system without and with warfarin was decreased from 28.6×10^5 to 3.6×10^5 L mol^{-1}, indicating that warfarin could significantly affect the binding of RAC to BSA. The above experimental results and analysis indicated that the binding of RAC to BSA mainly located within site I (sub-domain IIA).

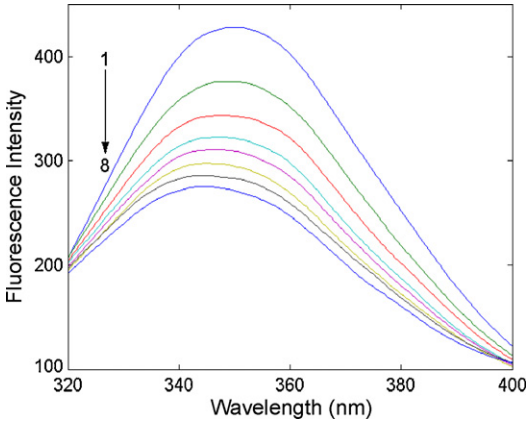

Fig. 5. The fluorescence spectra of the RAC/BSA system with the addition of warfarin. $r_{RAC:BSA} = 2$ ($c_{BSA} = 3.33 \times 10^{-8}$ mol L^{-1} and $c_{RAC} = 6.67 \times 10^{-8}$ mol L^{-1}), and $c_{warfarin}$ was added from 0 to 1.17×10^{-7} mol L^{-1} at 1.67×10^{-8} mol L^{-1} interval.

Table 3
The binding constants of warfarin/BSA system with the addition of RAC at 298 K.

$r_{warfarin:BSA}$	K_a ($\times 10^5$ L mol^{-1})
0	28.6
1	6.3
2	5.7
3	5.3
4	4.7
5	3.6

4. Conclusion

In this paper, the interaction between Ractopamine and BSA has been studied by fluorescence, UV–vis and FT-IR spectroscopy.

- Through conventional method, the intrinsic fluorescence of BSA was quenched by RAC through static quenching mechanism. The negative value of enthalpy change (ΔH) and positive value of entropy change (ΔS) indicated that the electrostatic and hydrophobic interactions played major roles in stabilizing the complex.
- A strong interaction force between the RAC and BSA molecules showed that the drug has a long stored time in blood plasma and a profound poisonous effect.
- For competition displacement, it appeared that the binding site of RAC on the protein was around site I. The micro-environment and conformation of BSA were demonstrated to be changed in the presence of RAC by SFS and FT-IR spectra.
- By MCR-ALS method, the simultaneous recovery of the concentration profiles (quantitative information) and the pure spectra (qualitative information) for the analyses was possible. It led to the successful extraction of the pure RAC, BSA and especially the RAC-BSA complex spectra from the overlapping spectra, which

is of particular significance, as the extraction of the RAC-BSA can further understand the mechanism of the interaction.

Acknowledgments

The authors gratefully acknowledge the financial support of this study by the National Natural Science Foundation of China (NSFC20562009) and the State Key Laboratory of Food Science and Technology of Nanchang University (SKLF-MB-200807 and SKLF-TS-200819).

References

[1] P.K. Crome, F.K. McKeith, T.R. Carr, D.J. Jones, D.H. Mowrey, J. Cannon, Effect of Ractopamine on growth performance, carcass composition, and cutting yields of pigs slaughtered at 107 and 125 kilograms, J. Anim. Sci. 74 (1996) 709–716.
[2] FDA, Freedom of information summary. Original new animal drug application. NADA 141–221. Available: http://www.fda.gov/cvm/FOI/141-221.pdf, 2003 (accessed 22.06.2006).
[3] S.L. Gruber, J.D. Tatum, T.E. Engle, K.J. Prusa, S.B. Laudert, A.L. Schroeder, W.J. Platter, Effects of Ractopamine supplementation and postmortem aging on longissimus muscle palatability of beef steers differing in biological type, J. Anim. Sci. 86 (2008) 205–210.
[4] L.Y. Zhang, B.Y. Chang, T. Dong, P.L. He, W.J. Yang, Z.Y. Yang, Simultaneous determination of Salbutamol, Ractopamine, and Clenbuterol in animal feeds by SPE and LC-MS, J. Colloid Interface Sci. 47 (2009) 324–328.
[5] T. Sakai, T. Hitomi, K. Sugaya, S. Kai, M. Murayama, T. Maitani, Determination method for Ractopamine in swine and cattle tissues using LC/MS, J. Food Hyg. Soc. Jpn. 48 (2007) 144–147.
[6] J.A. Baszczak, T. Grandin, S.L. Gruber, T.E. Engle, W.J. Platter, S.B. Laudert, A.L. Schroeder, J.D. Tatum, Effects of Ractopamine supplementation on behavior of British, Continental, and Brahman crossbred steers during routine handling, J, Anim. Sci. 84 (2006) 3410–3414.
[7] J. Jaumot, R. Gargallo, A. de Juan, R. Tauler, A graphical user-friendly interface for MCR-ALS: a new tool for multivariate curve resolution, Chemometr. Intell. Lab. Syst. 76 (2005) 101–110.
[8] http://www.ub.es/gesq/mcr/mcr.htm.
[9] T. Peter, All About Albumin: Biochemistry Genetics and Medical Applications, Academic Press, San Diego, CA, 1996, pp. 9–75.
[10] M. Garrido, F.X. Rius, M.S. Larrechi, Multivariate curve resolution-alternating least squares (MCR-ALS) applied to spectroscopic data from monitoring chemical reactions processes, Anal. Bioanal. Chem. 390 (2008) 2059–2066.
[11] H. Gampp, M. Maeder, C.J. Meyer, A.D. Zuberbühler, Calculation of equilibrium constants from multiwavelength spectroscopic data—III: model-free analysis of spectrophotometric and ESR titrations, Talanta 32 (1985) 1133–1139.
[12] W. Windig, J. Guilment, Interactive self-modeling mixture analysis, Anal. Chem. 63 (1991) 1425–1432.
[13] R. Tauler, A.K. Smilde, B.R. Kowalski, Selectivity, local rank, three-way data analysis and ambiguity in multivariate curve resolution, J. Chemometr. 9 (1995) 31–58.
[14] R. Bro, S. de Jong, A fast non-negativity-constrained least squares algorithm, J. Chemometr. 11 (1997) 393–401.
[15] Y.N. Ni, S.J. Su, S. Kokot, Small molecule-biopolymer interactions: ultraviolet–visible and fluorescence spectroscopy and chemometrics, Anal. Chim. Acta 628 (2008) 49–56.
[16] M. Vives, R. Gargallo, R. Tauler, Multivariate extension of the continuous variation and mole-ratio methods for the study of the interaction of intercalators with polynucleotides, Anal. Chim. Acta 424 (2000) 105–114.
[17] Y.J. Hu, Y. Liu, L.X. Zhang, R.M. Zhao, S.S. Qu, Studies of interaction between colchicine and bovine serum albumin by fluorescence quenching method, J. Mol. Struct. 750 (2005) 174–178.
[18] Y.J. Hu, Y. Liu, R.M. Zhao, Spectroscopic studies on the interaction between methylene blue and bovine serum albumin, J. Photochem. Photobiol. A 179 (2006) 324–329.
[19] J.R. Lakowicz, Principles of Fluorescence Spectroscopy, second ed., Plenum Press, New York, 1999, pp. 237–265.
[20] X.Z. Feng, R.X. Jin, Y. Qu, X.W. He, Studies on the ion effect on the binding interaction between HP and BSA, Chem. J. Chin. Univ. 17 (1996) 866–869.
[21] P.D. Ross, S. Subramanian, Thermodynamics of protein association reactions: forces contributing to stability, Biochemistry 20 (1981) 3096–3102.
[22] X.L. Han, P. Mei, Y. Liu, Q. Xiao, F.L. Jiang, R. Li, Binding interaction of quinclorac with bovine serum albumin: A biophysical study, Spectrochim. Acta Part A 74 (2009) 781–787.
[23] G.Z. Chen, X.Z. Huang, J.G. Xu, Z.Z. Zheng, Z.B. Wang, Methods of Fluorescence Analysis, vol. 2, Science Press, Beijing, 1990.
[24] J.N. Miller, Recent advances in molecular luminescence analysis, Proc. Anal. Div. Chem. Soc. 16 (1979) 203–208.
[25] B. Klajnert, M. Bryszewska, Fluorescence studies on PAMAM dendrimers interactions with bovine serum albumin, Bioelectrochemistry 55 (2002) 33–35.
[26] W.K. Surewicz, H.H. Mantsch, D. Chapman, Determination of protein secondary structure by Fourier-transform infrared spectroscopy—a critical assessment, Biochemistry 32 (1993) 389–394.
[27] J.H. Tang, F. Luan, X.G. Chen, Binding analysis of glycyrrhetinic acid to human serum albumin: fluorescence spectroscopy, FTIR, and molecular modeling, Bioorgan. Med. Chem. 14 (2006) 3210–3217.
[28] Y. Li, W. He, J. Liu, F. Sheng, Z. Hu, X. Chen, Binding of the bioactive component jatrorrhizine to human serum albumin, Biochim. Biophys. Acta 1722 (2005) 15–21.
[29] J.L. Breloff, M.D. Crothers, Equilibrium studies of ethidium–polynucleotide interactions, Biochemistry 20 (1981) 3547–3553.
[30] Y.Z. Zhang, B. Zhou, B. Zhang, Interaction of malachite green with bovine serum albumin: determination of the binding mechanism and binding site by spectroscopic methods, J. Hazard. Mater. 163 (2009) 1345–1352.
[31] G. Zhang, Q. Que, J. Pan, J. Guo, Study of the interaction between icariin and human serum albumin by fluorescence spectroscopy, J. Mol. Struct. 881 (2008) 132–138.
[32] G. Sudlow, D.J. Birkett, D.N. Wade, Further characterization of specific drug binding sites on human serum albumin, Mol. Pharmacol. 12 (1976) 1052–1061.
[33] X.M. He, D.C. Carter, Atomic structure and chemistry of human serum albumin, Nature 358 (1992) 209–215.